International Journal of Applied Earth Observation and Geoinformation 151 (2026) 105385

Contents lists available at ScienceDirect

International Journal of Applied Earth Observation and Geoinformation

journal homepage: www.elsevier.com/locate/jag

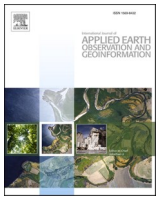

Mapping slash-and-burn in humid tropical rainforests based on Sentinel-1 imagery and 3D deep learning

Rui Sun [a,b], Feng Zhao [c,*], Carlos M. Souza Jr. [d], Ran Meng [e,f], Qihao Weng [a,b,g], Hanqin Tian [h,i], Jie Liu [e,f]

[a] JC STEM Lab of Earth Observations, Department of Land Surveying and Geo-Informatics, The Hong Kong Polytechnic University, Hung Hom, Hong Kong
[b] Research Centre for Artificial Intelligence in Geomatics, The Hong Kong Polytechnic University, Hung Hom, Kowloon, Hong Kong
[c] Key Laboratory of Sustainable Forest Ecosystem Management-Ministry of Education/College of Forestry, Northeast Forestry University, Harbin 150040, China
[d] Imazon—Amazonia People and Environment Institute, Belém, Pará, Brazil
[e] Artificial Intelligence Research Institute, Faculty of Computing, Harbin Institute of Technology, Harbin 150006, China
[f] State Key Laboratory of Smart Farm Technologies and Systems, Harbin, Heilongjiang 150006, China
[g] Research Institute for Land and Space, The Hong Kong Polytechnic University, Hung Hom, Kowloon, Hong Kong
[h] Department of Earth and Environmental Sciences, Boston College, Chestnut Hill, MA 02467, USA
[i] Center for Earth System Science and Global Sustainability, Boston College, Chestnut Hill, MA 02467, USA

ARTICLE INFO

Keywords:
Slash and burn
3D U-Net
Monthly mapping
Amazon fire

ABSTRACT

Intra-annual double disturbances (sequential disturbances occurring within a single year, such as slash-and-burn) in tropical regions result in more significant ecosystem impacts than single disturbances. However, optical data-based monitoring is limited by insufficient continuous spatio-temporal observations. Approaches using higher-frequency Sentinel-1 (S1) data, relying solely on temporal or spatial features, struggle to distinguish double disturbances due to noise and temporal heterogeneity. To address this issue, we propose an approach that employs a three-dimensional deep learning architecture to simultaneously extract multi-level embedded spatial context and temporal change characteristics—such as magnitude and duration features from time series S1 data to differentiate single and double disturbances. Additionally, we tested the effectiveness of incorporating an attention mechanism into the model to highlight key spatio-temporal features and suppress irrelevant information. The optimal model was applied to map double disturbances in three deforestation hotspot states in the Brazilian Amazon for 2019, identifying the first disturbance time at a monthly scale and verifying slash-and-burn by overlaying burned area maps. Results show that (1) the 3D U-Net model effectively extracted the spatio-temporal information of doubles disturbance in S1 data (F1 score of 0.912), and the integration of the attention mechanism highlighted distinctive temporal features, improving the balanced accuracy by 2.7%; (2) The optimal model (i.e., 3D U-Net with attention mechanism) exhibited potential generalization capability when mapping double disturbances in three states for 2019, with user's accuracy and producer's accuracy exceeding 0.85, and the estimated double disturbances area in three states in 2019 were 2685 ± 189 km^2; (3) 53.57% of mapped forest disturbances were double disturbances, 94.4% of which occurred outside the protected areas, highlighting the critical role of protected areas in ecological preservation. This study presents a novel S1-based framework for accurately characterizing intra-annual slash-and-burn events on a finer-grained spatial and temporal scale, providing useful information for carbon emission estimation and the development of effective conservation interventions.

1. Introduction

Forest loss in the tropics, particularly in the Amazon, has accelerated in recent decades due to intensified human activities and ongoing exploitation of tropical rainforests (Bourgoin et al., 2024; Flores et al., 2024). Double disturbances, such as slash-and-burn (Fig. 1a), can lead to more extreme ecological consequences than single disturbances (e.g., selective logging, clear-cut), significantly increasing the risk of soil

* Corresponding author.
E-mail address: fzhao@nefu.edu.cn (F. Zhao).

https://doi.org/10.1016/j.jag.2026.105385
Received 4 December 2025; Received in revised form 28 May 2026; Accepted 28 May 2026
Available online 1 June 2026

erosion, altering ecosystem resilience, and leading to more severe degradation (Buma, 2015; Kleinman et al., 2019; Seidl and Turner, 2022). Slash-and-burn is a widespread double disturbances in the tropics, primarily driven by agricultural expansion, often results in stand-replacing levels of canopy loss and is a key driver of long-term forest degradation (Brando et al., 2019; Chen et al., 2023; Daldegan et al., 2019; Tinker et al., 1996). However, burning after slashing often occurs swiftly, with time intervals ranging from one month to several months, which poses a significant challenge for continuous spatio-temporal monitoring. Thus, the spatio-temporal distribution of intra-annual slash-and-burn events in the Brazilian Amazon region remains unknown.

Compared with traditional ground-based field surveys, remote sensing technology offers advantages for large-scale dynamic forest monitoring (Fitts et al., 2022; Meng et al., 2017; Radeloff et al., 2024). In particular, optical data are widely used for detecting single disturbances on an inter-annual scale (Hansen et al., 2013; Senf and Seidl, 2021). However, clouds and shadows limit their ability to provide high-frequency, continuous observations, especially for detecting tropical intra-annual double disturbances at the monthly interval. Tang et al. (2023) reported that during the Amazon rainy season (February–April and November–December), monthly clear observations from Sentinel-2 do not fully cover the region. Several previous studies have used optical data to map single disturbances annually (e.g., logging, wildfire), and then overlapped the results with map products of another disturbance type (Nogueira Lisboa et al., 2024; Tao et al., 2019; Ye et al., 2021; Zhang et al., 2021). Nevertheless, when using optical data to monitor intra-year double disturbances such as slash-and-burn, achieving stable data coverage to support spatio-temporally continuous monitoring remains challenging.

Sentinel-1 (S1) data, with the ability to penetrate clouds and rain, is well-suited for timely mapping of disturbances within a year. Previous studies show that S1 data enhances the monitoring timeliness of forest disturbances such as forest harvesting (Zhao et al., 2022), fire (Belenguer-Plomer et al., 2019; Di Martino et al., 2023), and degradation (Balling et al., 2021; Bouvet et al., 2018; Fremout et al., 2022) through disturbance-induced reductions in canopy structure that weaken volume scattering and decrease radar backscatter coefficient (σ^o, typically expressed in dB) (Chuvieco et al., 2019; Tanase et al., 2015). Building on this mechanism, many pixel-based approaches analyze temporal trajectories of backscatter to identify disturbance signals, such as seasonal decomposition-based BFAST and harmonic regression-based CCDC. These methods were originally developed and validated on optical time series (e.g., Landsat), which typically benefit from high signal-to-noise ratios and stable temporal signals. However, when applied to Sentinel-1 SAR time series, pixel-level backscatter coefficients exhibit substantial fluctuations, leading to reduced accuracy and increased false alarms for disturbance (Hethcoat et al., 2021; Sun et al., 2023). While they show some capability for detecting disturbance events over multi-year time series, these approaches rely on specific

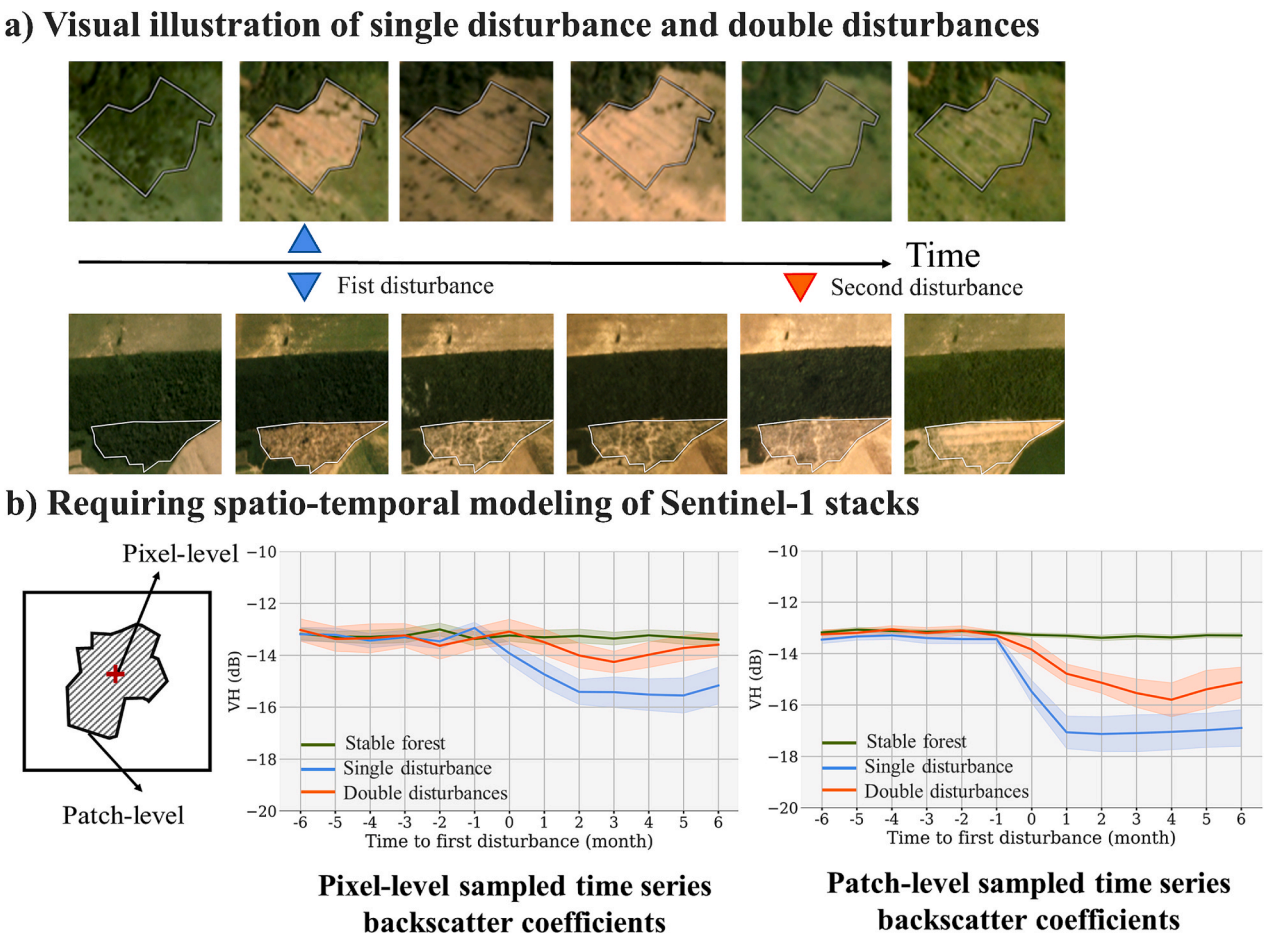

Fig. 1. A) visual representation illustrating the single disturbance(i.e., clear-cut) and double disturbances (i.e., slash-and-burn) activities in the tropics over time. Each panel includes a sequence of monthly PlanetScope composite images, where polygons represent manually delineated disturbance patches based on visual inspection. b) Example of a different level sampled S1 time series backscatter value. The patch level data takes the mean of the polygon, while the pixel level data takes the value of the center of the polygon. For each sampling level, the mean trajectory is shown with shaded areas indicating the 95% confidence interval (CI). The blue line represents single disturbance, and the red line represents double disturbances. (For interpretation of the references to colour in this figure legend, the reader is referred to the web version of this article.)

temporal modeling assumptions, where BFAST requires a recovery stage between abrupt changes for reliable trend fitting, and CCDC detects changes based on residual deviations from harmonic models (Bullock et al., 2022; Hethcoat et al., 2021). However, Intra-annual double disturbances occur over much shorter intervals than multi-year disturbances and lack a sufficiently long recovery. In Sentinel-1 SAR time series, backscatter does not decrease with successive disturbances but instead exhibits stage-dependent (Fig. 1b). For example, in slash-and-burn events, post-fire increases in surface roughness and residual char can elevate backscatter values and produce an apparent signal of recovery (Chuvieco et al., 2019). In addition, variability in disturbance intervals and severity, together with speckle noise, reduces the signal-to-noise ratio at the pixel level (Fig. 1b) (Ballère et al., 2021; De Luca et al., 2022; Sun et al., 2023). As a result, for these common pixel-based change detection approaches, the second disturbance signal is often weakened, smoothed during temporal fitting, or misclassified as noise or seasonal variability, and cannot be reliably resolved as a distinct disturbance event.

To reduce pixel-level noise, some studies incorporated spatial context, such as patch-level features or boundary effects, improving robustness for mapping single disturbances (Ballère et al., 2021; Zhao et al., 2022, 2026). However, methods that rely solely on spatial features remain lack the temporal context necessary to identify intra-annual double disturbances. Subsequent time-series strategies do not fully resolve this limitation, such as fixed moving windows (Tang et al., 2023) or Bayesian-based updating (Sun et al., 2023)—prioritize trajectory smoothing or recursive probability accumulation rather than explicitly modeling multi-phase disturbance dynamics. Consequently, when disturbance signals in backscatter overlap with seasonal variability or moisture-driven fluctuations, fixed-window smoothing may merge adjacent anomalies, while Bayesian updating may accumulate disturbance probability without event reset, leading to conflation or misattribution of intra-annual double disturbances. Instead, integrating spatio-temporal information, which incorporates both neighborhood context and temporal variation signatures, enables a more comprehensive characterization of dynamic changes and holds promise for advancing intra-annual double disturbances detection (Cardille et al., 2022; Tang et al., 2023).

Recently, deep learning-based methods (Md Jelas et al., 2024; Mullissa et al., 2023; Solórzano et al., 2023), especially three-dimensional (3D) convolution-based deep learning approaches, present a promising approach to S1-based forest disturbance monitoring by extracting complex features end-to-end (Dixon et al., 2023; Hashemi et al., 2024). Compared with 1D (pixel-based) or 2D convolution (single-scene), the 3D convolution kernel operates across both spatial and temporal dimensions, preserving the 3D structure of the data. By using larger receptive fields, 3D convolution-based deep learning methods can capture multi-scale change patterns while reducing the spatio-temporal semantic information loss of subtle change caused by feature separation (Isaienkov et al., 2021; Masolele et al., 2021). Existing studies have demonstrated that 3D convolutional methods significantly improve the monitoring of single disturbance at yearly intervals. For example, Dixon et al. (2023) used a 3D CNN to map canopy mortality induced by wildfires, and Solórzano et al. (2023) used a 3D U-Net combined with synthetic aperture radar (Sentinel-1) and multi-spectral images (Sentinel-2) to detect deforestation.

However, the ability of 3D convolutional methods to improve the accuracy of mapping forest intra-annual double disturbances using time series S1 data has not been explored. Unlike single-event disturbances, double disturbances involve temporally proximate events with varying intervals and durations, introducing strong temporal heterogeneity that may challenge model generalization. It is unclear whether 3D convolutional methods alone can effectively highlight critical spatio-temporal information associated with double disturbances. Moreover, previous studies have shown that attention mechanism enable models to adaptively focus on informative spatial regions and temporal steps based on input characteristics (e.g., tree species, crop type, and inland water bodies) (Huang et al., 2023; Li et al., 2025; Oktay et al., 2018), allowing more effective feature selection and providing an opportunity to explicitly capture disturbance interval and duration information in intra-annual double disturbances.

Thus, we aim to map intra-annual double disturbances at the monthly scale by fully utilizing the spatio-temporal features of S1 data with a novel 3D convolutional structure and attention mechanism, which may also provide a framework for other tropical regions and for different types of temporally successive intra-annual disturbances beyond the Amazonian slash-and-burn scenario, such as consecutive fires within a year or fire followed by logging. We propose the following research questions:

1) To what extent can the 3D convolution-based deep learning method detect and differentiate single and double disturbances using spatio-temporal signals of time series S1 data?
2) Does incorporating the attention mechanism further enhance the capability of the model to detect key temporal patterns of double disturbances (e.g., disturbance intervals and intensity changes), and what improvements in overall accuracy and balanced accuracy can it achieve over the baseline model?
3) What are the temporal and spatial distribution characteristics of intra-annual double disturbances among hotspots of the Brazilian Amazon rainforests in the year 2019?

2. Study area and Materials

2.1. Study area

Brazil, the largest country in South America, is home to vast forest resources, notably in the Amazon Basin, which contains two-thirds of the Amazon rainforest. Forest cover in Brazil is approximately 4,079,827 km^2, or 48% of the total area (https://mapbiomas.org) (Fig. 2). Most areas of the country have a tropical climate, characterized by high temperatures and substantial rainfall, particularly during the rainy season (December–May) with monthly precipitation of 200–300 mm and temperatures averaging 25 °C–30 °C. The dry season (June–November) sees lower rainfall (50–100 mm) and temperatures between 28 °C and 35 °C (Wright et al., 2017). Forests in Brazil, especially in the Amazon, have been significant, with 7,900 km^2 lost in 2018 due to agriculture, logging, mining, and fires (Curtis et al., 2018; Davidson et al., 2012; Pišl et al., 2024). This study focuses on three deforestation hotspots—Acre, Rondônia, and Pará— selected among the top ten tree cover loss states in Brazil since 2000 (Global Forest Watch). Although permanent agriculture expansion dominates across all three states, the relative contributions of fire and shifting cultivation vary, reflecting distinct frontier dynamics (Sun et al., 2023), providing heterogeneous disturbance contexts to evaluate the generalization of the proposed model and to analyze intra-annual double disturbances at the state level.

2.2. Materials

2.2.1. Global forest change product

This study utilized the Global Forest Change product (version 1.9) (Hansen et al., 2013) to exclude non-forest areas and get forest extent in 2018. This Landsat-based product provides annual forest loss at 30 m resolution from 2000 to 2019 via Google Earth Engine (GEE). Forests were defined as areas with a tree cover of at least 30% and a tree height of at least 5 m. Additionally, forest loss in 2019 was used as a criterion for determining whether reference labels include annual forest loss (see Section 3.1).

2.2.2. Fire monitor product

To identify fire events contributing to forest loss, we used the

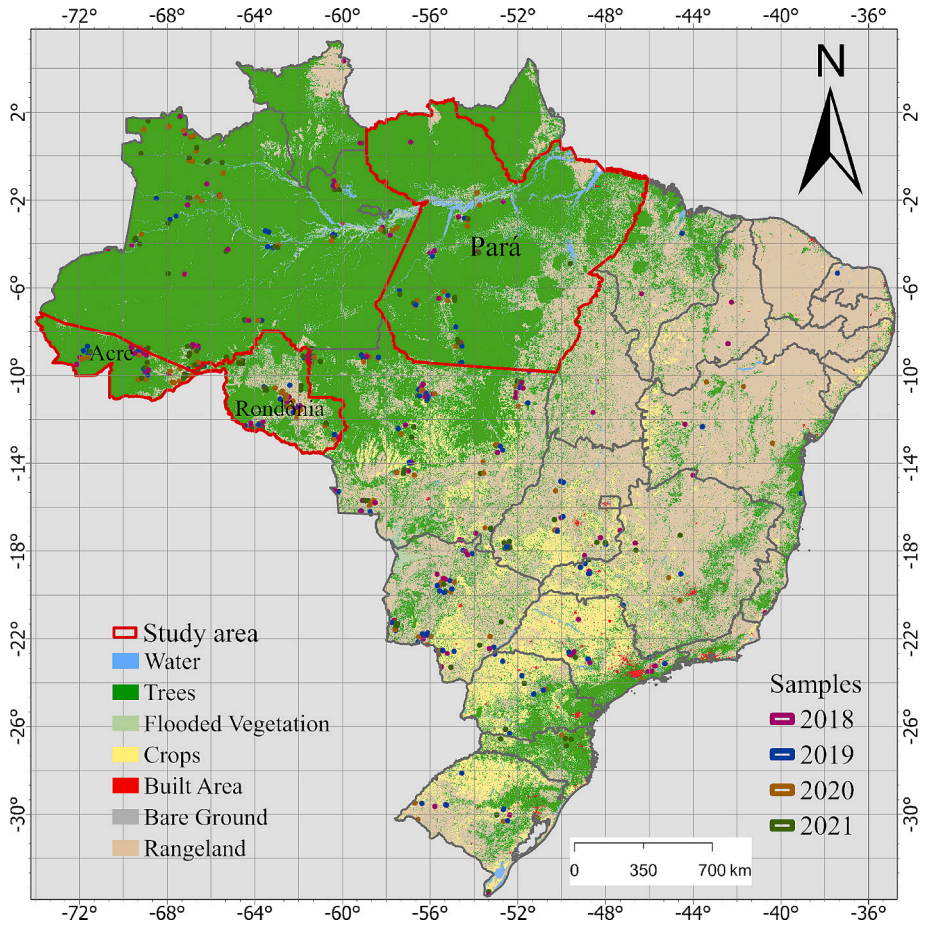

Fig. 2. Study areas in Brazil, land cover map is derived from the ESRI 10 m Annual Land Cover (2017) product (Karra et al., 2021). All samples for training, testing, and validation are displayed in four colors by year. Note: Each sample has a size of 128-by-128 S1 pixels.

monthly Fire Monitor fire product (https://brasil.mapbiomas.org/en/dados-monitor-mensal-do-fogo/). This dataset provides monthly fire maps derived from Landsat imagery (30 m, 1985–2018) and, since 2019, from Sentinel-2 imagery (10 m), offering consistent, high-resolution fire monitoring across Brazil. We used this dataset to determine the timing of burning events and support identifying double disturbances and fire-related single disturbances.

2.2.3. Reference data

Reference data were derived from monthly PlanetScope composites (https://www.planet.com), with 575 forest disturbance samples manually labeled from 2018 to 2021 (Fig. 2), mainly in the Amazon biome. Each sample covered a 128 by 128 pixels patch of S1 data, equivalent to 1.28 km by 1.28 km. To generate these samples, we identified candidate sites by randomly selecting 200 points per year within annual forest loss areas mapped by the Global Forest Change product, with sampling probability proportional to the spatial distribution of mapped forest loss. Around each point, a 640 m buffer rectangle was created, and rectangles with forest loss areas smaller than 1,000 m^2 (i.e., 10 S1 pixels) were excluded to minimize spatial uncertainty from the Global Forest Change product (approximately 1 pixel at 30 m resolution) and avoid unstable detections due to limited C-band sensitivity and speckle noise at very small patch sizes. For each valid rectangle, the month with the most obvious forest loss was selected, and polygon tools were used to delineate disturbed areas (such as vegetation cover change, the appearance of bare land, or darker areas) (Fig. 1a). Double disturbances were further identified by examining changes within the same year (e.g., burned surfaces after logging) using fire monitoring products (Section 2.2.2). Each polygon was labeled by the month of the first disturbance: single events as 1–12 and double events as 13–24. Approximately 140 samples per year were retained (148, 144, 142, and 141 for 2018, 2019, 2020, and 2021, respectively), ensuring a uniform monthly distribution across 2018–2021 (exact number of samples per month is shown in Fig. S1).

2.3. Sentinel-1 data

The Sentinel-1 synthetic aperture radar (SAR) C-band (5.405 GHz) data were acquired from Google Earth Engine and preprocessed using the Sentinel-1 Toolbox (Mullissa et al., 2020; Vitale et al., 2021). Due to the different revisit intervals of the Sentinel-1A and Sentinel-1B, both ascending and descending orbits were used to maximize monthly coverage. The final S1 input images had a spatial resolution of 10 m and included dual-polarization bands (VV and VH). A 1000-meter inward buffer was applied along the Sentinel-1 scene boundary to mitigate potential border noise artifacts, with the buffer distance empirically determined based on visual inspection of scene edges. A 13-scene monthly composite S1 stack spanning December of the previous year through December of the current year was generated using the mean value for each month. No additional denoising filters were applied, as multi-temporal composites have been shown to effectively reduce single-date speckle (Mullissa et al., 2020; Vitale et al., 2021).

3. Methods

The methodological framework is divided into 1) Image preprocessing and sampling, 2) 3D convolutional deep learning modeling, 3) Model evaluation, and 4) Regional double disturbances mapping and analysis.

3.1. Image pre-processing and sampling

To analyze the temporal sensitivity of Sentinel-1 backscatter to forest disturbances, 267 polygon samples representing stable forest, single disturbance, and double disturbances classes were selected (Section 2.2.3). Monthly VH backscatter was extracted from composite images at both pixel-level and patch-level scales for six months before and after the first disturbance. For model training, 13-scene S1 stacks spanning from December of the previous year to December of the disturbance year were sampled based on the reference labels. We cross-checked the manually annotated monthly disturbance labels against the Global Forest Change annual forest loss product to ensure that each sample reflected only the labeled month of disturbance. Samples were cropped to 32-by-32 S1 pixels to reduce temporal mismatch caused by multiple disturbance months within the original 128-by-128 patches, and retained only when the overlap between monthly labels and annual forest loss exceeded 90% (examples of the different types of reference data are shown in Supplementary Fig. S2), a threshold determined by comparing manually interpreted patch boundaries from monthly PlanetScope composites with the Hansen 30 m forest loss product, which effectively mitigates boundary misalignment errors while preserving representative samples for training (sensitivity analysis of the overlap threshold is shown in Supplementary Fig. S3). Finally, 90% of the sampled dataset was used for training (see training, testing, and validation sets in Table S1), with the remaining 10% reserved for generalization evaluation (see Section 3.3.2).

3.2. Training models

3.2.1. 3D deep neural network classifiers

The three baseline models used in this study are: (1) 3D convolutional neural networks (3D CNN), which employs stacked 3*3*3 convolution layers with 2*2*2 max pooling, processing two spectral bands (VH, VV) and progressively increasing channels from 32 to 128 (Fig. S4a). The network consists of three convolutional blocks, each including two 3D convolutional layers followed by Batch Normalization, ReLU activation, and max-pooling, with dropout applied after each block. A fully connected layer is used before the final softmax output for classification, and the model contains approximately 7.97 million parameters. This architecture captures both spatial and temporal features through volumetric convolutions (Fu et al., 2022; Gallo et al., 2023; Sagan et al., 2021); (2) Convolutional Long Short-Term Memory (convLSTM) networks consists of two ConvLSTM layers with 64 hidden units each, integrating 3*3 spatial convolutions with recurrent LSTM units (Fig. S4b). The model takes the full temporal sequence as input, where temporal dependencies are captured and propagated through the internal LSTM gating mechanisms (i.e., input, forget, and output gates) across time steps. The first layer preserves the sequential information, while the second layer aggregates it into a compact spatio-temporal representation. A 2D convolutional layer with a softmax activation is applied at the output to generate classification maps (Cai et al., 2023; Chamorro Martinez et al., 2021); and (3) 3D U-Net (Fig. S4c), which uses an encoder-decoder architecture to extract multi-scale hierarchical features for volumetric data (Çiçek et al., 2016). The encoder consists of two convolutional blocks with 32 and 64 filters, respectively, each of which includes two 3D convolutional layers, with batch normalization and max-pooling applied after each layer. The bottleneck layer contains two 3D convolutional layers with 128 filters. ReLU is used throughout the hidden layers, while a softmax activation is applied at the output to generate class probabilities.

3.2.2. 3D u-net with attention gate

The Attention Gate (AG) is a mechanism used in deep learning models that directs the focus of model toward important feature regions while suppressing irrelevant background or noise, demonstrating strong effectiveness in remote sensing image segmentation (Jamali et al., 2023; John and Zhang, 2022). The fundamental concept of AG is to compute a weight coefficient matrix from the input feature maps using attention-like operations, typically via a multi-layer perceptron (MLP) or convolutional layers, to assign varying weights across positions. In this study, we implemented a voxel-wise spatiotemporal attention gate within the 3D U-Net framework, where volumetric feature maps (time*height*width) are refined through attention gates applied at skip connections (Fig. 3) prior to feature fusion. Specifically, the attention weights are computed by first projecting the decoder feature map and the corresponding encoder feature map into a common feature space using 3*3*3 convolutions. The projected features are then summed and passed through a ReLU activation, followed by a 3*3*3 convolution to generate a single-channel attention map. A sigmoid activation is subsequently applied to obtain normalized attention coefficients, resulting in a voxel-wise attention map that is multiplied element-wise with the encoder features.

3.2.3. Model training parameters

To train 3D deep learning models, several parameters were adopted (see Table S2 for key parameter settings). The model was trained using classification cross-entropy as the loss function, with Adam adopted as the optimizer and learning rate was set to 0.001. Considering the convergence degree of the model, the training epoch of iterations for updating model weights was set to 100. For each epoch, batch size was set to 16 to help balance computational efficiency and training stability. In addition, to mitigate overfitting and avoid redundant computation, early stopping was set to 10 epochs, stopping training when the loss of validation data did not improve for 10 continuous epochs.

3.3. Accuracy assessments

3.3.1. Assessment of deep neural network classifiers

Model performance was assessed using five widely adopted accuracy metrics: overall accuracy (OA), user's accuracy (UA), producer's accuracy (PA), and the F1 score. Additionally, balanced accuracy was applied for a more comprehensive evaluation, given that the disturbance classification at the monthly scale in this study involved multiple classes.

$$OA = \frac{TP + TN}{TP + TN + FP + FN} \tag{1}$$

$$UA = \frac{TP}{TP + FP} \tag{2}$$

$$PA = \frac{TP}{TP + FN} \tag{3}$$

$$F1 = \frac{2*UA*PA}{UA + PA} = \frac{2TP}{2TP + FP + FN} \tag{4}$$

$$BalancedAccuracy = \frac{1}{C}\sum_{i=1}^{C}\frac{TP_i}{TP_i + FN_i} \tag{5}$$

where TP, TN, FP, FN represent true positive, true negative, false positive, and false negative, respectively. C represents the total classes of classified double disturbances map, and i represents each class.

3.3.2. Evaluations of model generalization among three hotspot places

To compare the regional prediction performance and generalizability of different modeling methods, we selected 50 independent validation samples (32-by-32 S1 pixels per sample, see 3.1; the distribution of the 50 samples across the three regions is provided in Table S3) from three deforestation hotspot states: (a) Acre, (b) Rondônia, (c) Pará. In addition, a 30 km by 30 km area in each state was selected to represent and compare the double disturbances mapping results of different methods.

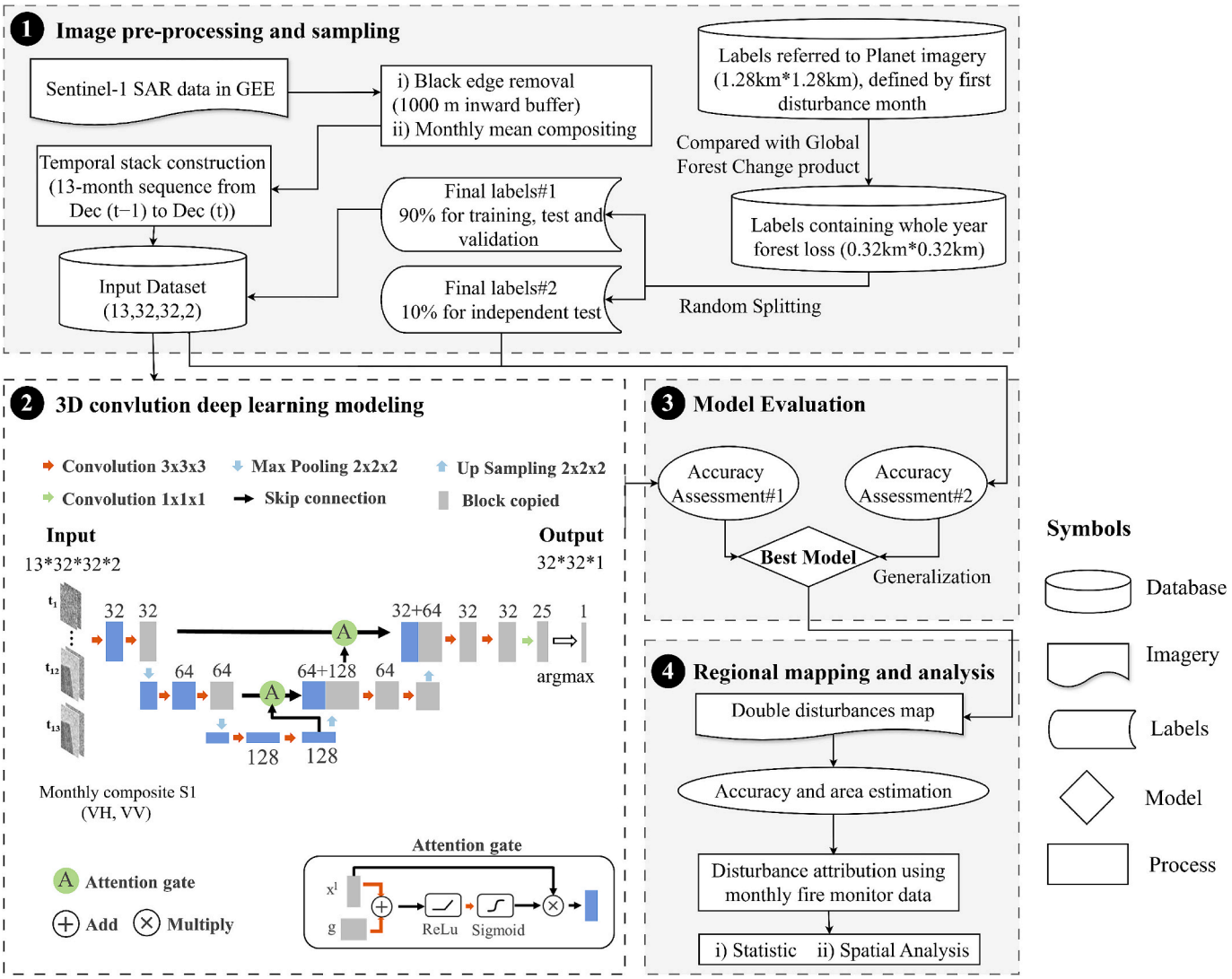

Fig. 3. The workflow of this study.

3.3.3. Double disturbances map generation and accuracy estimation

Double disturbances map for the three states were generated using the 13-scene monthly S1 composite stack spanning December 2018 to December 2019 and the optimized 3D deep learning model. Temporal gaps in the 13-scene monthly S1 stacks (Fig. S5) were filled via linear interpolation to maintain consistent time-series input for model prediction (Li, 2020; Liu et al., 2024). Map accuracy was evaluated following recommended guidelines (Olofsson et al., 2014), using stratified random sampling to select approximately 2,000 pixels per region. This approach enabled estimation of class-specific accuracy and area (stable forest, single disturbance, double disturbances), accounting for both sample size and class proportions.

3.4. Double disturbances map analysis

The double disturbances monitoring map for 2019 in Acre, Rondônia, and Pará was analyzed, using monthly fire maps (i.e., MapBiomas Fire Monitor) to verify fire occurrence within single (i.e., forest fire) and double disturbances (i.e., slash-and-burn). Considering the time lag between the two data sources, pixels where fires occurred only before or after a disturbance by two months can be classified as fire-related single disturbances. For double disturbances, fires occurring in the month of the first disturbance or later are counted as slash-and-burn. Disturbance areas were aggregated on 50 km by 50 km grids to balance landscape heterogeneity and regional representativeness. Restricted areas, such as Indigenous lands, were overlaid to assess protected area effectiveness in limiting forest disturbances (https://geoserver.funai.gov.br/geoserver/web/) (Cortinhas Ferreira Neto et al., 2024).

4. Results

4.1. Changes in Sentinel-1 SAR backscatter coefficients of double disturbances

Fig. 1b shows the pixel-level and patch-level S1 monthly composites for the stable forest, single disturbance, and double disturbances. Temporal VH backscatter at the patch level showed higher separability between disturbance types. For stable forests, the VH backscatter coefficient remained consistently around −13 to −13.5 dB. In contrast, temporal VH backscatter coefficients of other two types of disturbance decreased after the first disturbance, reflecting changes in canopy structure or surface roughness. For single disturbance, the mean value of the VH backscatter coefficient of at patch-level showed a significant decrease within one month before and after the disturbance, dropping from approximately − 13.5 to − 17 dB. In the following months, the VH backscatter coefficient remained relatively stable, with a less obvious upward trend. For double disturbances, the mean VH backscatter coefficient at patch-level decreased by approximately 1.3 dB (from − 13.5 to

− 14.8 dB) within one month after the first disturbance, followed by a further decline of about 1.0 dB to a minimum of − 15.8 dB over the subsequent months. In addition, the VH backscatter coefficient of double disturbances rebounded relatively quickly in the months following the lowest point compared to a single disturbance.

4.2. Accuracy assessments

Based on the validation dataset in final labels #1, the performance of four 3D deep learning methods was evaluated. Fig. 4a compares the accuracy in classifying 25 disturbance classes at a monthly scale. The 3D U-Net model achieved higher performance than the 3D CNN and convLSTM, with an overall accuracy of 0.89 and an F1 score of 0.89, respectively. Considering class proportions, the balanced accuracy decreased to 0.85, 0.81, and 0.77, for 3D U-Net, 3D CNN, and convLSTM, respectively. Incorporating the Attention Gate module into the 3D U-Net further improved performance, notably increasing balanced accuracy by 0.03 (see Table S4 for class-wise results, with more than half of the classes reaching the highest accuracy among all compared models). Among the remaining models, 3D CNN consistently outperformed convLSTM. As shown in Fig. 4b, when disturbance classes were aggregated into three categories—single disturbance, double disturbances, and others— the 3D U-Net with the Attention Gate achieved the highest performance, with all metrics around 0.913. The 3D U-Net model performed slightly worse, while convLSTM outperformed the 3D CNN across all metrics, achieving an F1 score of 0.874.

4.3. Performance of model generalization

Fig. 5 shows the disturbance classification accuracy (UA and PA) of different models across regions and classes. Panels a–c present 25-class classification considering both first disturbance time and disturbance type, while panels d–f show 3-class classification based on disturbance type only. In general, the 3D U-Net model and the 3D U-Net model with the attention gate module outperformed other models, with UA and PA above 0.825 (Detailed statistical significance analysis is provided in the Fig. S6). In Acre, the 3D U-Net model achieved a UA of 0.873 and a PA of 0.862 for 25-class, and 0.881 for both metrics in three-class classification. In Rondônia, UA and PA of 3D U-Net model were 0.864 and 0.825 for 25-class, and 0.857 and 0.859 for 3-class classification. In Pará, the 3D U-Net model with the attention gate module slightly outperformed the 3D U-Net model, with UA and PA values of 0.875 and 0.860 for 25-class, and 0.879 for both metrics in 3-class. Additionally, for 25-class classification, the 3D CNN model outperformed the convLSTM model in all three states, whereas the convLSTM model was more accurate than the 3D CNN in 3-class classification in Acre and Pará.

Fig. 6 shows the annual global forest change product, the fire within forest loss product, and regional predictions from four models. Most forest loss in the three hotspot regions overlaps with fire events, primarily between September and November. For classifying disturbances at different times (Fig. 6a), the 3D U-Net and 3D U-Net models with an attention gate module show higher accuracy and consistency with the annual forest loss product, while the convLSTM and 3D CNN models have higher misclassification rates, particularly in November and December. Fig. 6b displays the classification results for single and double disturbances. The convLSTM model has the highest omissions, especially for large patches in Pará. The 3D CNN model misclassifies single disturbance and others, while the 3D U-Net model performs best, with higher accuracy for both disturbance types, though it still misses double disturbances in Pará. The attention gate further reduces misclassification of small patches.

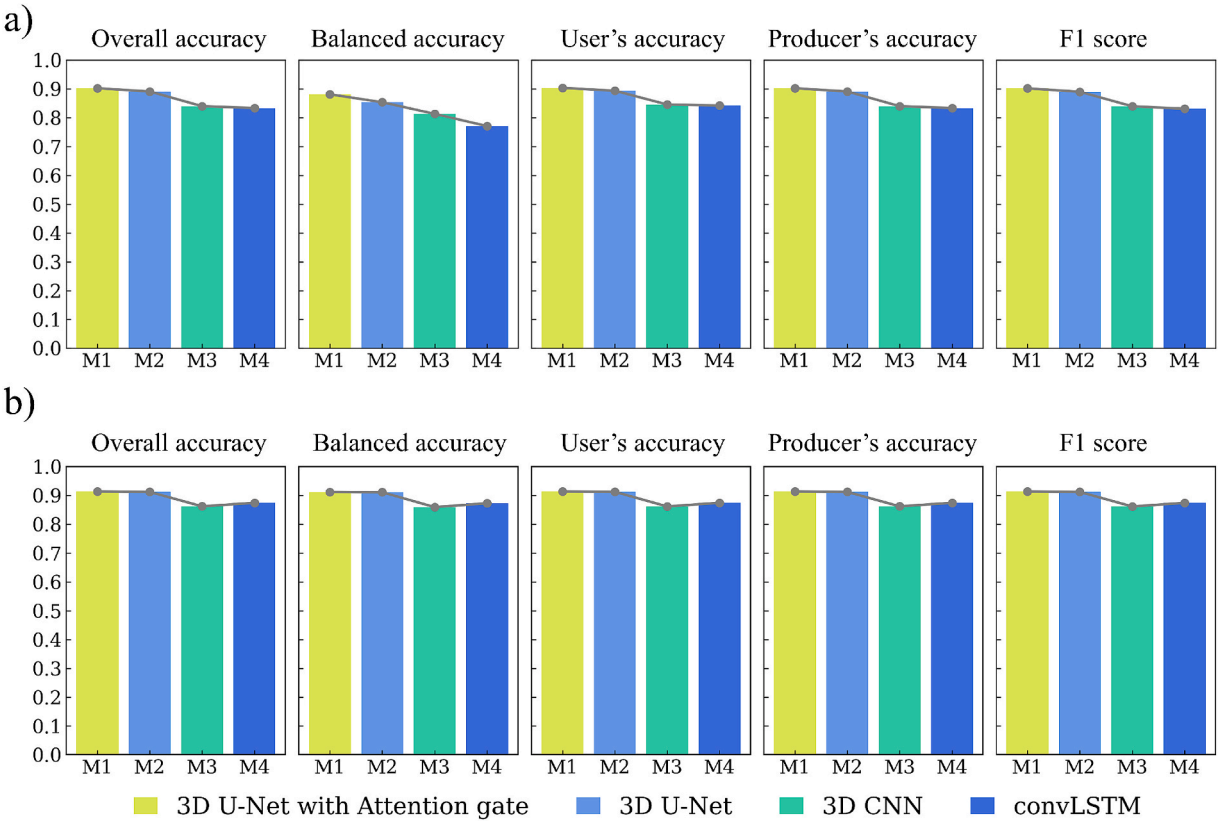

Fig. 4. Accuracy assessment of classification models. a) Classification of 25 classes considered both the first disturbance time and the disturbance type. b) Classification of 3 classes considered only the disturbance type. M1-M4 refers to four tested deep learning models.

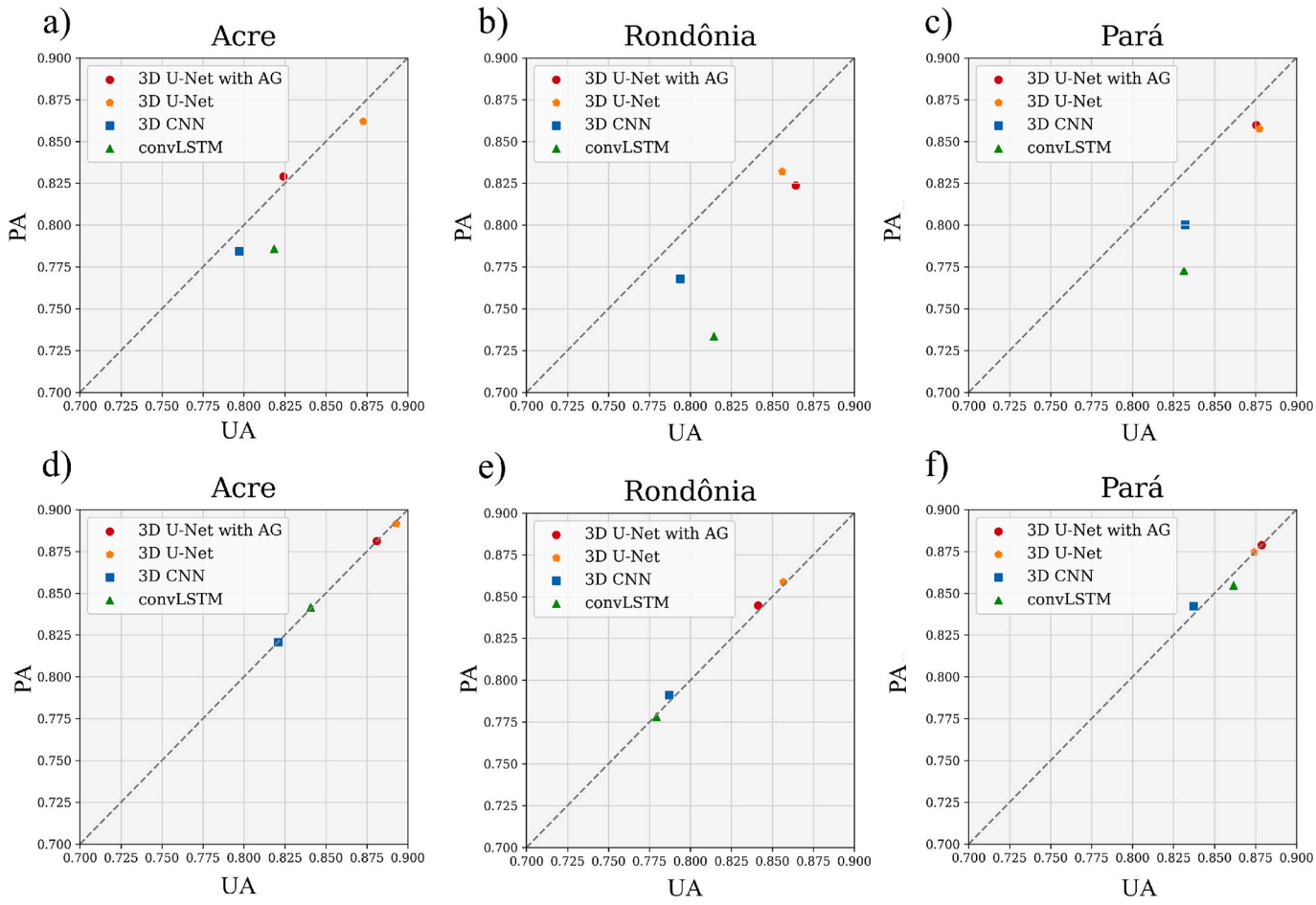

Fig. 5. Validation of the model among three areas. a), b), c): Classification of 25 classes considered both the first disturbance time and type. d), f) g): Classification of 3 classes considered only disturbance type.

4.4. Double disturbances mapping and analysis in 2019

Using the best method (i.e., the 3D U-Net model with the addition of the attention gate module) together with monthly composite S1 images, we generated double disturbances maps for the three states in 2019 (Fig. 7). More than 90% of the forest disturbance in Acre is concentrated in the dry season (June to September), with double disturbances exceeding 55%. Rondônia showed higher distribution from January to May, peak above 300 km^2 in August. In Pará, forest disturbance remained below 100 km^2 from January to May, except for April, then steadily increased from May to August, exceeding 600 km^2 in August and September, while the proportion of double disturbances declined after September, particularly in November.

The accuracy and area of regional double disturbances maps were estimated (Table S5) with 95% confidence intervals. The proportions of single and double disturbances were relatively low in all three states. In Acre and Pará, UA and PA exceeded 0.92, with estimated areas slightly larger than mapped areas. In Rondônia, a considerable portion of single disturbance was misclassified as double disturbances, resulting in lower UA for double disturbances and an underestimation of single disturbance (769 ± 95 km^2), indicating a tendency of the model to over-detect multi-phase disturbance signals due to the temporal similarity between single and compound disturbances and the complex disturbance dynamics in the region. Across the three states, the estimated area of single disturbance was 2920 ± 210 km^2, while that of double disturbances was 2685 ± 189 km^2.

4.5. Fire-related disturbance analysis

In 2019, fire-related double disturbances (slash-and-burn) accounted for over 65% of the total double disturbances area across Acre, Rondônia, and Pará (Fig. 8). In Acre and Rondônia, slash-and-burn dominated between June and September, representing over 70% of double disturbances, peaking at 95.18% in Rondônia in July (Fig. 8a and b). In Pará, it accounted for over 50% of double disturbances, except in January, February, and December (Fig. 8c). For single disturbances (Fig. 8d, e and f), forest fire loss accounted for less than 35% of the total disturbed area in all three states. In Acre, forest fire loss contributed 96% of annual fire losses between June and September, while in Rondônia and Pará, forest fires contributed 80% and 68% of annual losses, respectively, during the dry season (July–November).

As shown in Fig. 9, the annual forest disturbance area of all grids in Acre is less than 30 km^2, with half dominated by fire-related disturbances. In Rondônia, one-quarter of the grids have an annual forest disturbance greater than 10 km^2, and these grids entirely dominated by fire-related disturbances. In Pará, one-third of grids were fire-dominated, but over half of grids above 10 km^2 were non-fire single disturbances. In addition, most grids with large forest disturbance areas, especially those dominated by fire-related disturbance, were outside of the restricted areas.

5. Discussion

Our study provides a novel framework for directly monitoring intra-annual double disturbances such as slash-and-burn in tropical regions at

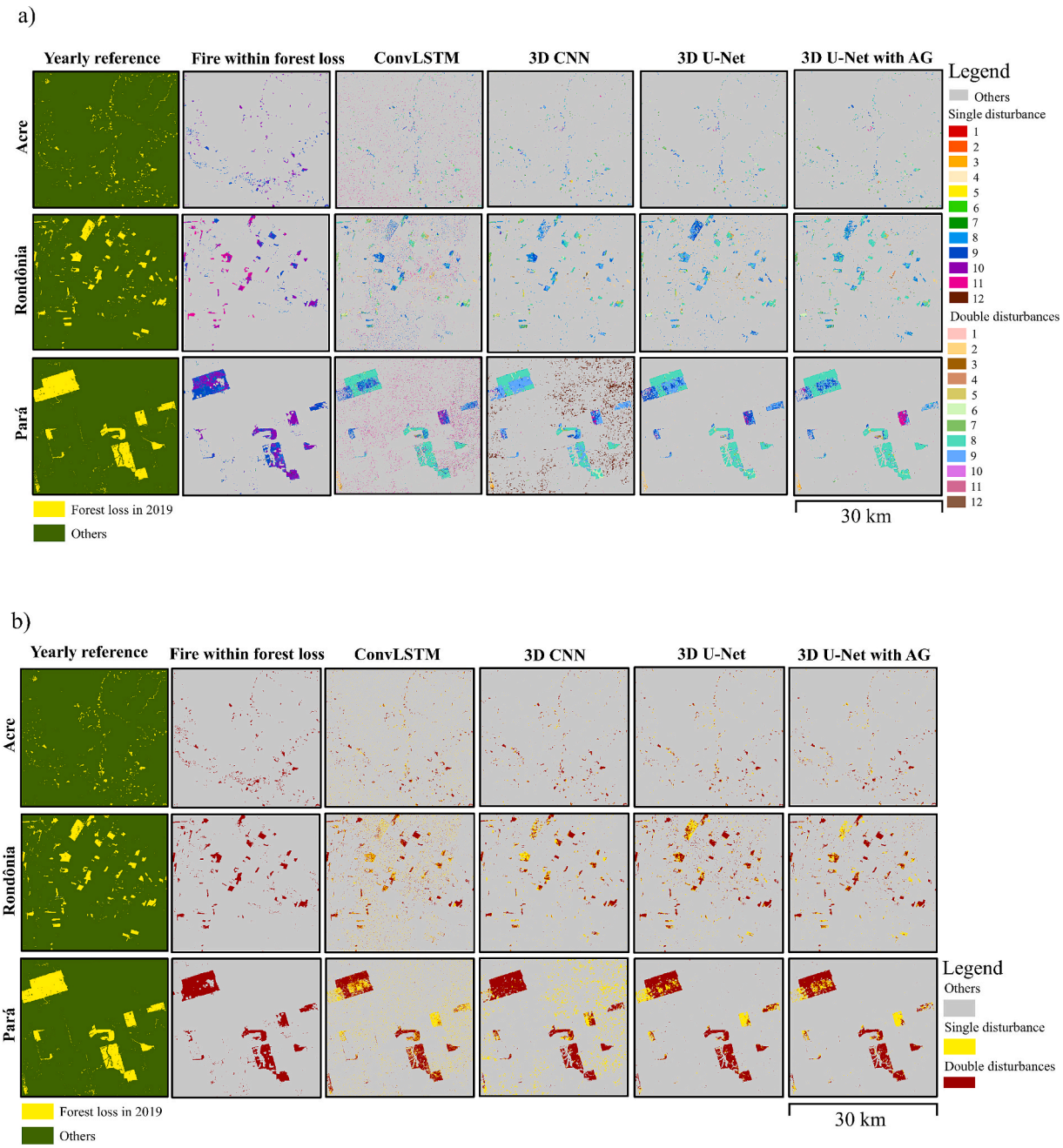

Fig. 6. Detailed double disturbances maps in three hotspots in 2019. a) Classification of 25 classes considered both disturbance types and the first disturbance time. b) Classification of 3 classes considered only disturbance types.

a monthly scale. Specifically, a 3D deep learning network was used to simultaneously and effectively extract the spatio-temporal features of double disturbances in time series S1 data. and accurately characterizing intra-annual slash-and-burn events on a finer-grained spatial and temporal scale. Through this framework, it is able to accurately characterize intra-annual slash-and-burn events on a finer-grained spatial and temporal scale. Below we will discuss the challenge of timely monitoring double disturbances (5.1), the performance of the proposed 3D U-Net model for S1 based monthly double disturbances mapping (5.2), and implications and future studies (5.3).

5.1. Challenges for timely monitoring of intra-annual double disturbances

Previous studies have tended to either provide high-accuracy annual monitoring of continuous disturbances or focus on near-real-time detection approaches with relatively coarse spatial detail (Chen et al., 2023; Meng et al., 2022; Stahl et al., 2023), but monitoring intra-annual double disturbances (e.g., slash-and-burn in tropics, and usually happen within several months) presents greater challenges (Le Page et al., 2010). High observation frequency is needed to avoid omission, while dynamic signal changes from varying disturbance severity and timing add complexity (McGregor et al., 2024).

The monitoring of S1-based intra-annual double disturbances is further complicated by the uncertain intervals between sequential events and the similarity of short-term backscatter responses between slash-and-burn and deforestation, leading to ambiguous detection (Cardille et al., 2022; Dutra et al., 2022). To address these challenges, we propose an approach that integrates a 3D convolutional architecture with an attention mechanism to adaptively highlight critical signals and suppress irrelevant features from the time series S1 data. Our results

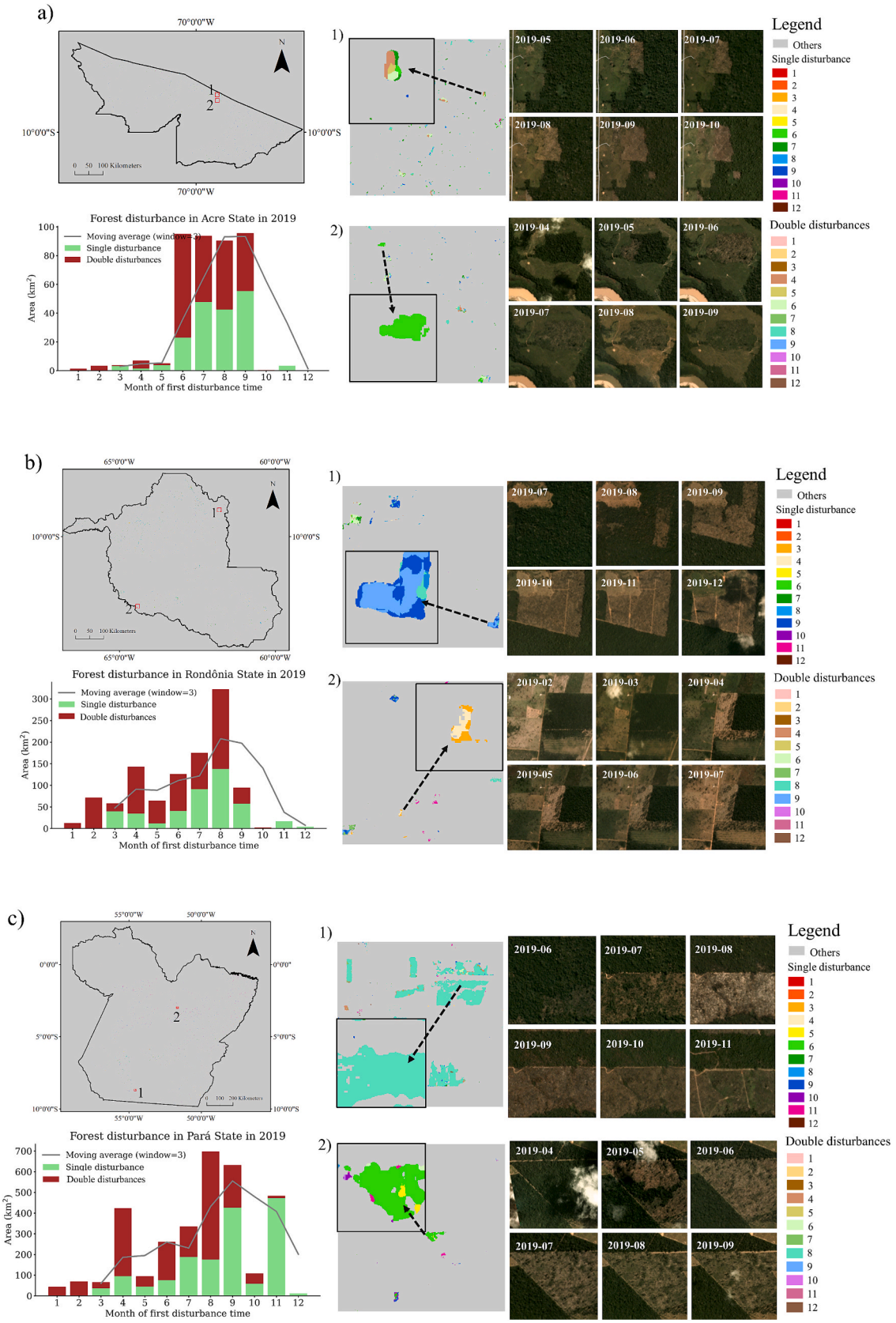

Fig. 7. Forest disturbance maps in 2019 for a) Acre state; b) Rondônia state; c) Pará state. Two red square areas are displayed with a separate zoom-in view for each study area, 1) mainly shows the double disturbances area, and 2) mainly shows the single disturbance area. Right next to the four zoom-in view windows are high-resolution monthly mosaic images for the months before and after the first disturbance time, respectively, obtained from the Planet CubeSat. (For interpretation of the references to colour in this figure legend, the reader is referred to the web version of this article.)

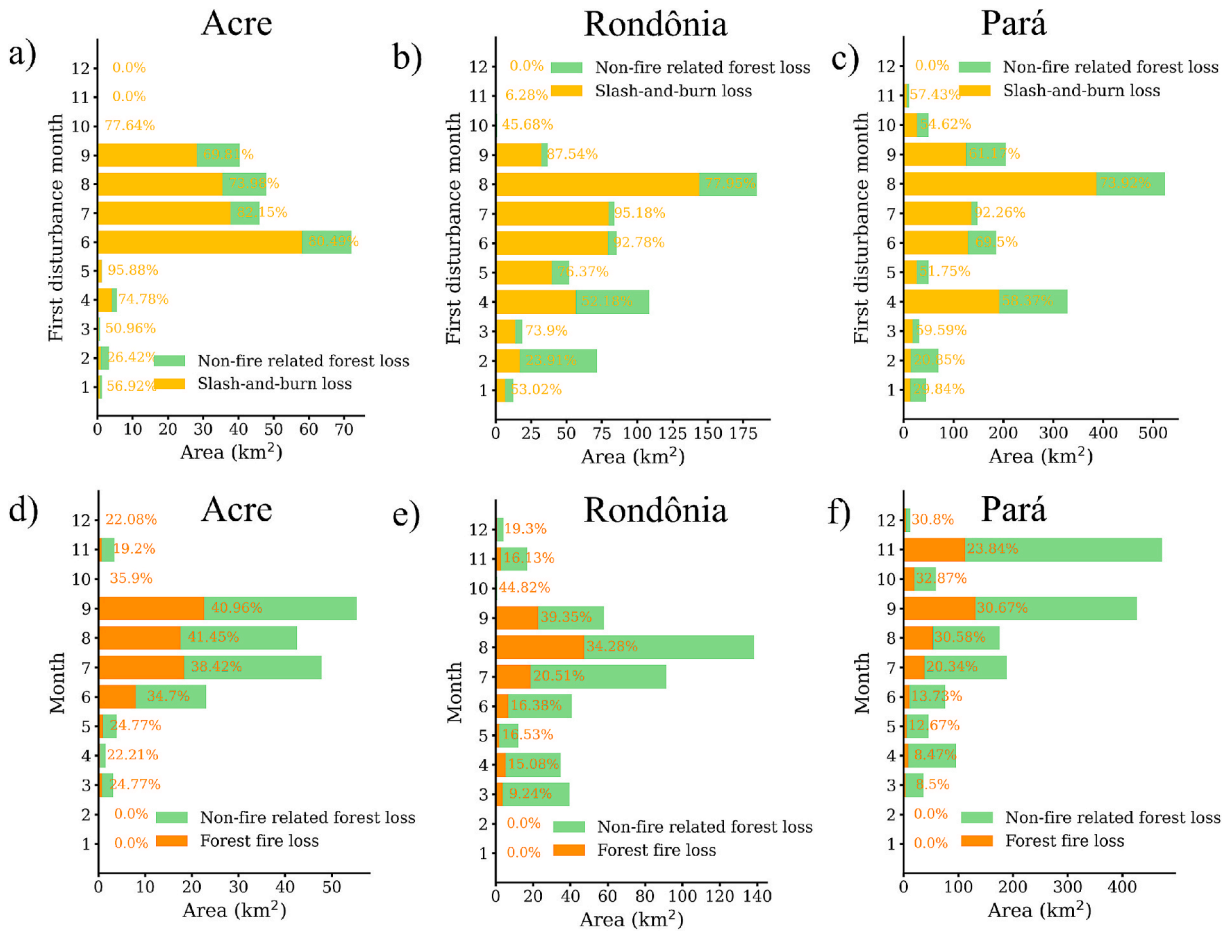

Fig. 8. Fire-related disturbance statistics in 2019. a), b), c): Areas and proportions of slash-and-burn in double disturbances. d), e), f): areas and proportions of forest fire in single disturbances.

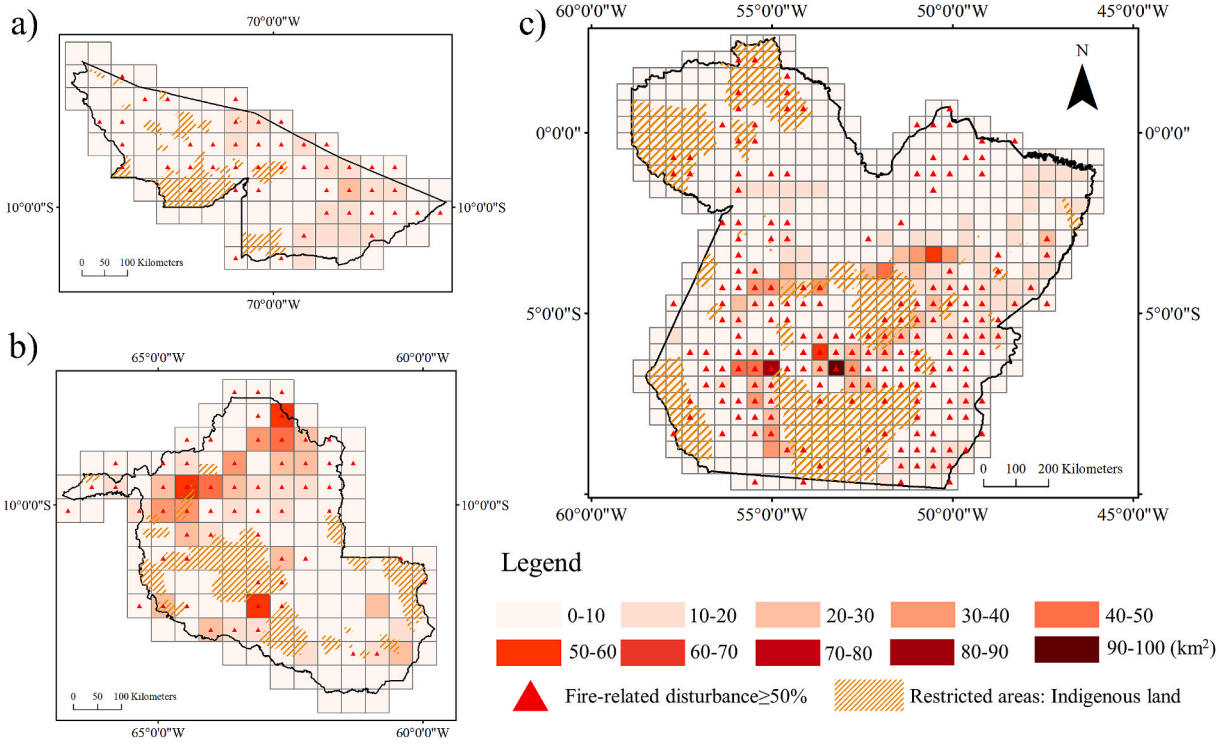

Fig. 9. Forest disturbance maps in 2019, shown as the sum values within 50 km by 50 km grid. a) Acre; b) Rondônia; c) Pará.

show robust and generalizable performance in timely mapping of intra-annual double disturbances in tropical forests. This study presents a novel attempt to use intelligent algorithm mapping intra-annual slash-and-burn from radar data, providing a new perspective on monitoring timeliness and enhancing characterization of intra-annual double events (such as drought-induced forest fire, salvage logging, slash-and-burn), particularly under intensifying climate change and human pressures (Bullock et al., 2020; Dunn et al., 2019).

5.2. Performance of the proposed 3D u-net model for S1-based intra-annual double disturbances mapping

To explore the attention weights of different models across single and double disturbances, Fig. S7 shows the spatio-temporal attention weights of the 3D U-Net and 3D U-Net with attention gate module in prediction results, temporal attention weights, and class activation maps. The attention-enhanced 3D U-Net model provided more accurate predictions and focused on key temporal features, filtering out irrelevant information. Grad-CAM analysis revealed that the attention model produced more coherent activation patterns, improving the delineation of disturbance areas and separating single and double disturbances more clearly.

To examine the separability of high-dimensional features extracted by different models, we exported the penultimate layer predictions for the validation set, randomly selecting 5,000 pixel-level samples and using t-SNE for dimensionality reduction (Fig. 10). The average Euclidean distances (D1 and D2) were calculated to assess intra- and inter-class distances. The t-SNE visualization showed that the convLSTM model had the highest D1 and lowest D2, exhibiting mixed and dispersed features. The 3D CNN captured spatio-temporal patterns better, forming structured clusters. The 3D U-Net showed improved feature extraction, but with some overlap. The 3D U-Net with attention mechanism (AG) achieved the clearest separation, with compact clusters and the highest D2, demonstrating superior feature discrimination and highlighting the benefits of attention mechanisms in distinguishing double disturbances.

To assess the transferability of the proposed approach, an additional experiment was conducted in a region of Bolivia (without any training data for this region), where wildfires play a relatively larger role in forest loss compared with the three Brazilian states. Following the same sampling strategy, an independent validation dataset of 50 patches (32-by-32 S1 pixels) corresponding to 2019 forest disturbances was randomly generated based on the spatial distribution of the Global Forest Loss product (Fig. S8a). The 3D U-Net with attention mechanism (AG) model achieved an overall accuracy of 0.71 for identifying double disturbances, and an accuracy of 0.683 for distinguishing disturbance timing when allowing a tolerance of one month (Fig. S8b). Furthermore, regional mapping over a 30 km by 30 km area (Fig. S9) shows that the 3D U-Net combined with the attention gate provides the most accurate forest loss detection and the clearest boundary delineation among the tested models, suggesting that the framework possesses a certain degree of transferability to regions with different disturbance drivers.

We assessed the influence of disturbance intervals on double disturbances monitoring by reclassifying validation samples in Section 3.4 into three groups based on the calendar time (in months) between the first and second detected disturbance events: (1) intervals shorter than three months, (2) intervals between three and seven months, and (3) intervals longer than seven months. Fig. 11 shows that the highest accuracy was achieved for intervals of 3–7 months, with an overall

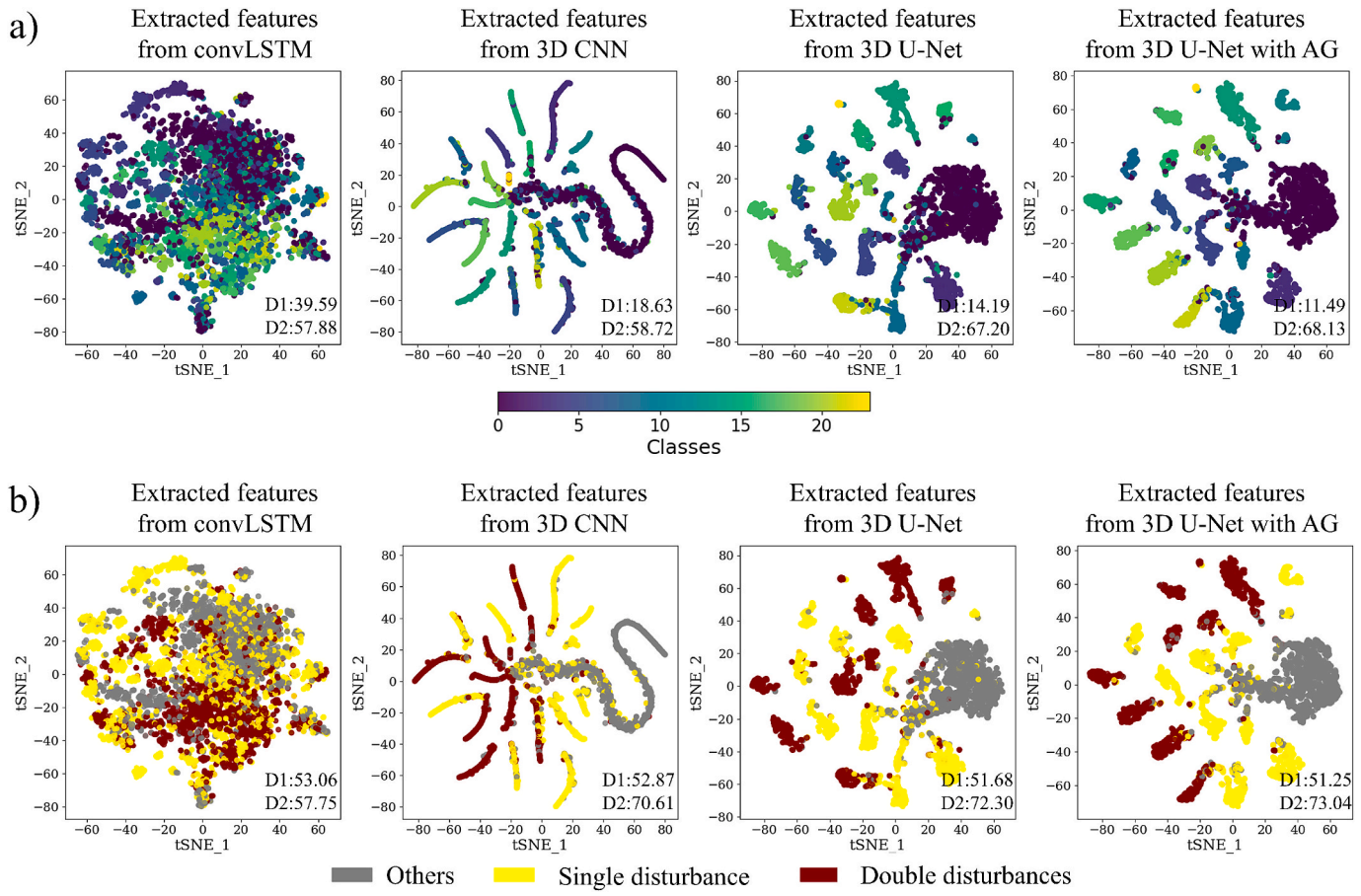

Fig. 10. Comparison of feature separability using t-SNE visualization of two-dimensional features from second-to-last layer of each model. D1: average intra-class distance; D2: average inter-class distance. When the intra-class distance (D1) is smaller and the inter-class distance (D2) is larger, the model clustering effect is better. a) Distinguishing 25 classes considered both disturbance type and first disturbance time. b) Distinguishing 3 classes considered only disturbance type.

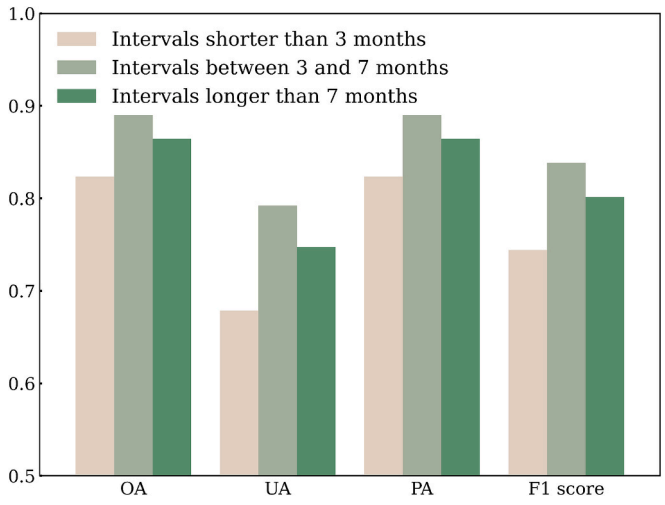

Fig. 11. Accuracy assessment of double disturbances with different intervals.

accuracy of 0.89 and F1 score of 0.84. For intervals longer than 7 months, accuracy decreased slightly (overall accuracy 0.85, F1 score 0.80). The lowest accuracy was observed for intervals shorter than 3 months, with an overall accuracy of 0.82 and F1 score of 0.74. Therefore, model performance is expected to be higher in regions where intra-annual double disturbances are typically separated by more than three months.

5.3. Implications and future studies

This study considered the impact of forest disturbance type and the first disturbance time at a finer temporal (monthly) and spatial (10-meter) scale, providing valuable insights for ecological research and forest management. Finer-scale maps of double disturbances, particularly for slash-and-burn, are critical for more accurate carbon emission estimation, as fires occurring immediately after logging often result in incomplete combustion due to high fuel moisture and limited drying time, whereas fires following a longer interval allow fuel desiccation and accumulation, leading to more efficient combustion (Brando et al., 2019; Yu and Ginoux, 2022). Accurate monitoring of disturbance timing and type can aid in assessing ecological consequences, such as vegetation recovery during the rainy season, which promotes seed bank protection and enhances fire resistance (Smith et al., 2023). In addition, the mapping highlighted that fire-related disturbances were largely outside protected areas, underscoring the importance of effective forest management (Cortinhas Ferreira Neto et al., 2024).

The within-year double disturbances we monitored in this study were primarily related to the two major drivers of forest disturbance in the Brazilian Amazon—fire and deforestation—typically occurring within a single year. Potential cases of three or more disturbances, such as those arising from an interaction of natural and anthropogenic factors (e.g., drought or hurricanes followed by multiple fires) (Feng et al., 2021), were not further examined due to high canopy-scale uncertainty. Beyond this, the availability of high-quality reference samples for intra-annual double disturbances remains limited. Identifying disturbance timing and types requires careful interpretation of high-temporal-resolution imagery, making large-scale annotation labor-intensive. Although a sensitivity analysis demonstrated that model performance gradually stabilizes when the number of training samples exceeds 700 patches (Fig. S10), suggesting that the current dataset is sufficient to support reliable model training, the limited sample diversity may still constrain the ability of the model to capture the full variability of disturbance patterns. For example, the lack of samples smaller than 1,000 m^2 may lead to misclassification or under-detection of very small-scale disturbances. In addition, variations in topography, forest types, and disturbance regimes may influence the applicability and performance of the proposed model. For future work, multi-source remote sensing data—including optical data (such as Sentinel-2 and Planetscope) and radar data (such as ALOS-2 PALSAR-2 and GEDI) sources—combined with large-scale AI models, could be integrated through data fusion strategies to enhance spectral and structural information representation (Lu and Weng, 2026). Approaches such as SAR–optical translation and multi-source data fusion may further increase temporal observation density, thereby improving spatial–temporal coverage (Fig. S5) and the reliability of double disturbances monitoring results, while emerging Transformer-based architectures such as Vision Transformers (ViT) may further enhance the modeling of complex spatio-temporal disturbance dynamics once larger training datasets become available (Slagter et al., 2024; Tian et al., 2025). In our supplementary experiment, a Swin Transformer-based model (Liu et al., 2021) outperformed the 3D CNN and convLSTM baselines but remained less accurate than the 3D U-Net and attention-gated 3D U-Net under the current Sentinel-1 training dataset (Table S6 and Fig. S11). This suggests that Transformer-based models are promising for future intra-annual disturbance monitoring, but may require larger labeled SAR datasets, stronger regularization, or self-supervised pretraining to fully exploit their representation capacity.

6. Conclusions

This study proposed a 3D deep learning approach for monitoring intra-annual double disturbances in tropical forests based on time-series Sentinel-1 data. Among the tested architectures, the 3D U-Net achieved the best performance by leveraging multi-scale feature fusion and spatio-temporal contextual information, while the integration of an attention mechanism further improved accuracy and generalization by adaptively suppressing redundant signals. Results show that more than half of intra-annual double disturbances events in three hotspot states of the Amazon were fire-related disturbances, most of which are outside of the protected areas. The fine-scale double disturbances maps derived from this approach provide critical information for carbon emission estimation, biodiversity conservation, and evaluating the ecological impacts of tropical forest disturbances under climate change, thereby supporting the development of more effective management and policy interventions.

CRediT authorship contribution statement

Rui Sun: Writing – review & editing, Writing – original draft, Software, Methodology, Formal analysis, Conceptualization. **Feng Zhao:** Writing – review & editing, Supervision, Project administration, Methodology, Funding acquisition, Conceptualization. **Carlos M. Souza:** Writing – review & editing, Visualization, Investigation. **Ran Meng:** Writing – review & editing, Supervision, Resources, Methodology, Conceptualization. **Qihao Weng:** Writing – review & editing, Validation, Resources. **Hanqin Tian:** Writing – review & editing. **Jie Liu:** Writing – review & editing.

Declaration of competing interest

The authors declare that they have no known competing financial interests or personal relationships that could have appeared to influence the work reported in this paper.

Acknowledgements

We thank the three anonymous reviewers for their constructive feedback. Thanks to Yanyan Shen and Ping Zhao for their help with sample preparation. This work was supported by National Natural Science Foundation of China (No. 42371395); Dr. Ran Meng was supported by National Natural Science Foundation of China (No. 42471362) and

the Key Research and Development Program of Heilongjiang, China (grant No. 2022ZX01A25; No. JD2023GJ01).

Appendix A. Supplementary data

Supplementary data to this article can be found online at https://doi.org/10.1016/j.jag.2026.105385.

Data availability

Data will be made available on request.

References

Ballère, M., Bouvet, A., Mermoz, S., Le Toan, T., Koleck, T., Bedeau, C., André, M., Forestier, E., Frison, P.-L., Lardeux, C., 2021. SAR data for tropical forest disturbance alerts in French Guiana: Benefit over optical imagery. Remote Sens. Environ. 252. https://doi.org/10.1016/j.rse.2020.112159.

Balling, J., Verbesselt, J., De Sy, V., Herold, M., Reiche, J., 2021. Exploring archetypes of tropical fire-related forest disturbances based on dense optical and radar satellite data and active fire alerts. Forests 12. https://doi.org/10.3390/f12040456.

Belenguer-Plomer, M.A., Tanase, M.A., Fernandez-Carrillo, A., Chuvieco, E., 2019. Burned area detection and mapping using Sentinel-1 backscatter coefficient and thermal anomalies. Remote Sens. Environ. 233. https://doi.org/10.1016/j.rse.2019.111345.

Bourgoin, C., Ceccherini, G., Girardello, M., Vancutsem, C., Avitabile, V., Beck, P.S.A., Beuchle, R., Blanc, L., Duveiller, G., Migliavacca, M., Vieilledent, G., Cescatti, A., Achard, F., 2024. Human degradation of tropical moist forests is greater than previously estimated. Nature 631, 570–576. https://doi.org/10.1038/s41586-024-07629-0.

Bouvet, A., Mermoz, S., Ballère, M., Koleck, T., Le Toan, T., 2018. Use of the SAR shadowing effect for deforestation detection with Sentinel-1 time series. Remote Sens. 10, 1250.

Brando, P.M., Silverio, D., Maracahipes-Santos, L., Oliveira-Santos, C., Levick, S.R., Coe, M.T., Migliavacca, M., Balch, J.K., Macedo, M.N., Nepstad, D.C., Maracahipes, L., Davidson, E., Asner, G., Kolle, O., Trumbore, S., 2019. Prolonged tropical forest degradation due to compounding disturbances: implications for CO(2) and H(2) O fluxes. Glob. Chang. Biol. 25, 2855–2868. https://doi.org/10.1111/gcb.14659.

Bullock, E.L., Healey, S.P., Yang, Z., Houborg, R., Gorelick, N., Tang, X., Andrianirina, C., 2022. Timeliness in forest change monitoring: a new assessment framework demonstrated using Sentinel-1 and a continuous change detection algorithm. Remote Sens. Environ. 276, 113043.

Bullock, E.L., Woodcock, C.E., Souza Jr, C., Olofsson, P., 2020. Satellite-Based Estimates Reveal Widespread Forest Degradation in the Amazon. Glob. Change Biol. n/a. DOI: 10.1111/gcb.15029.

Buma, B., 2015. Disturbance interactions: characterization, prediction, and the potential for cascading effects. Ecosphere 6, 1–15. https://doi.org/10.1890/es15-00058.1.

Cai, Z., Hu, Q., Zhang, X., Yang, J., Wei, H., Wang, J., Zeng, Y., Yin, G., Li, W., You, L., Xu, B., Shi, Z., 2023. Improving agricultural field parcel delineation with a dual branch spatiotemporal fusion network by integrating multimodal satellite data. ISPRS J. Photogramm. Remote Sens. 205, 34–49. https://doi.org/10.1016/j.isprsjprs.2023.09.021.

Cardille, J.A., Perez, E., Crowley, M.A., Wulder, M.A., White, J.C., Hermosilla, T., 2022. Multi-sensor change detection for within-year capture and labelling of forest disturbance. Remote Sens. Environ. 268. https://doi.org/10.1016/j.rse.2021.112741.

Chamorro Martinez, J.A., Cué La Rosa, L.E., Feitosa, R.Q., Sanches, I.D., Happ, P.N., 2021. Fully convolutional recurrent networks for multidate crop recognition from multitemporal image sequences. ISPRS J. Photogramm. Remote Sens. 171, 188–201. https://doi.org/10.1016/j.isprsjprs.2020.11.007.

Chen, S., Olofsson, P., Saphangthong, T., Woodcock, C.E., 2023. Monitoring shifting cultivation in Laos with Landsat time series. Remote Sens. Environ. 288. https://doi.org/10.1016/j.rse.2023.113507.

Chuvieco, E., Mouillot, F., van der Werf, G.R., San Miguel, J., Tanase, M., Koutsias, N., García, M., Yebra, M., Padilla, M., Gitas, I., Heil, A., Hawbaker, T.J., Giglio, L., 2019. Historical background and current developments for mapping burned area from satellite Earth observation. Remote Sens. Environ. 225, 45–64. https://doi.org/10.1016/j.rse.2019.02.013.

Çiçek, Ö., Abdulkadir, A., Lienkamp, S.S., Brox, T., Ronneberger, O., 2016. 3D U-Net: learning dense volumetric segmentation from sparse annotation. Presented at the Medical Image Computing and Computer-Assisted Intervention–MICCAI 2016: 19th International Conference, Athens, Greece, October 17-21, 2016, Proceedings, Part II 19, Springer, pp. 424–432.

Cortinhas Ferreira Neto, L., Diniz, C.G., Maretto, R.V., Persello, C., Silva Pinheiro, M.L., Castro, M.C., Sadeck, L.W.R., Filho, A.F., Cansado, J., Souza, A.A.A., Feitosa, J.P., Santos, D.C., Adami, M., Souza-Filho, P.W.M., Stein, A., Biehl, A., Klautau, A., 2024. Uncontrolled Illegal Mining and Garimpo in the Brazilian Amazon. Nat Commun 15, 9847. DOI: 10.1038/s41467-024-54220-2.

Curtis, P.G., Slay, C.M., Harris, N.L., Tyukavina, A., Hansen, M.C., 2018. Classifying drivers of global forest loss. Science 361, 1108–1111. https://doi.org/10.1126/science.aau3445.

Daldegan, G.A., Roberts, D.A., Ribeiro, F. de F., 2019. Spectral mixture analysis in Google Earth Engine to model and delineate fire scars over a large extent and a long time-series in a rainforest-savanna transition zone. Remote Sens. Environ. 232. DOI: 10.1016/j.rse.2019.111340.

Davidson, E.A., de Araújo, A.C., Artaxo, P., Balch, J.K., Brown, I.F., C. Bustamante, M.M., Coe, M.T., DeFries, R.S., Keller, M., Longo, M., 2012. The Amazon basin in transition. Nature 481, 321–328.

De Luca, G., Silva, J.M.N., Modica, G., 2022. Short-term temporal and spatial analysis for post-fire vegetation regrowth characterization and mapping in a Mediterranean ecosystem using optical and SAR image time-series. Geocarto Int. 37, 15428–15462. https://doi.org/10.1080/10106049.2022.2097482.

Di Martino, T., Le Saux, B., Guinvarc'h, R., Thirion-Lefevre, L., Colin, E., 2023. Detection of Forest Fires through Deep Unsupervised Learning Modeling of Sentinel-1 Time Series. ISPRS Int. J. Geo-Inf. 12. DOI: 10.3390/ijgi12080332.

Dixon, D.J., Zhu, Y., Brown, C.F., Jin, Y., 2023. Satellite detection of canopy-scale tree mortality and survival from California wildfires with spatio-temporal deep learning. Remote Sens. Environ. 298. https://doi.org/10.1016/j.rse.2023.113842.

Dunn, C.J., O'Connor, C.D., Reilly, M.J., Calkin, D.E., Thompson, M.P., 2019. Spatial and temporal assessment of responder exposure to snag hazards in post-fire environments. For. Ecol. Manag. 441, 202–214. https://doi.org/10.1016/j.foreco.2019.03.035.

Dutra, D.J., Anderson, L.O., Fearnside, P.M., Graça, P.M.L. de A., Yanai, A.M., Dalagnol, R., Burton, C., Jones, C., Betts, R., Aragão, L.E.O. e C. de, 2022. Fire Dynamics in an Emerging Deforestation Frontier in Southwestern Amazonia, Brazil. Fire 6. DOI: 10.3390/fire6010002.

Feng, X., Merow, C., Liu, Z., Park, D.S., Roehrdanz, P.R., Maitner, B., Newman, E.A., Boyle, B.L., Lien, A., Burger, J.R., Pires, M.M., Brando, P.M., Bush, M.B., McMichael, C.N.H., Neves, D.M., Nikolopoulos, E.I., Saleska, S.R., Hannah, L., Breshears, D.D., Evans, T.P., Soto, J.R., Ernst, K.C., Enquist, B.J., 2021. How deregulation, drought and increasing fire impact amazonian biodiversity. Nature 597, 516–521. https://doi.org/10.1038/s41586-021-03876-7.

Fitts, L.A., Domke, G.M., Russell, M.B., 2022. Comparing methods that quantify forest disturbances in the United States' national forest inventory. Environ. Monit. Assess. 194. https://doi.org/10.1007/s10661-022-09948-z.

Flores, B.M., Montoya, E., Sakschewski, B., Nascimento, N., Staal, A., Betts, R.A., Levis, C., Lapola, D.M., Esquivel-Muelbert, A., Jakovac, C., Nobre, C.A., Oliveira, R.S., Borma, L.S., Nian, D., Boers, N., Hecht, S.B., Ter Steege, H., Arieira, J., Lucas, I.L., Berenguer, E., Marengo, J.A., Gatti, L.V., Mattos, C.R.C., Hirota, M., 2024. Critical transitions in the Amazon forest system. Nature 626, 555–564. https://doi.org/10.1038/s41586-023-06970-0.

Fremout, T., Cobián-De Vinatea, J., Thomas, E., Huaman-Zambrano, W., Salazar-Villegas, M., Limache-de la Fuente, D., Bernardino, P.N., Atkinson, R., Csaplovics, E., Muys, B., 2022. Site-specific scaling of remote sensing-based estimates of woody cover and aboveground biomass for mapping long-term tropical dry forest degradation status. Remote Sens. Environ. 276. https://doi.org/10.1016/j.rse.2022.113040.

Fu, H., Shao, Z., Fu, P., Huang, X., Cheng, T., Fan, Y., 2022. Combining ATC and 3D-CNN for reconstructing spatially and temporally continuous land surface temperature. Int. J. Appl. Earth Obs. Geoinformation 108. https://doi.org/10.1016/j.jag.2022.102733.

Gallo, I., Ranghetti, L., Landro, N., La Grassa, R., Boschetti, M., 2023. In-season and dynamic crop mapping using 3D convolution neural networks and sentinel-2 time series. ISPRS J. Photogramm. Remote Sens. 195, 335–352. https://doi.org/10.1016/j.isprsjprs.2022.12.005.

Hansen, M.C., Potapov, P.V., Moore, R., Hancher, M., Turubanova, S.A., Tyukavina, A., Thau, D., Stehman, S.V., Goetz, S.J., Loveland, T.R., 2013. High-resolution global maps of 21st-century forest cover change. Science 342, 850–853.

Hashemi, M.G.Z., Jalilvand, E., Alemohammad, H., Tan, P.-N., Das, N.N., 2024. Review of synthetic aperture radar with deep learning in agricultural applications. ISPRS J. Photogramm. Remote Sens. 218, 20–49. https://doi.org/10.1016/j.isprsjprs.2024.08.018.

Hethcoat, M.G., Carreiras, J.M., Edwards, D.P., Bryant, R.G., Quegan, S., 2021. Detecting tropical selective logging with C-band SAR data may require a time series approach. Remote Sens. Environ. 259, 112411.

Huang, Z., Zhong, L., Zhao, F., Wu, J., Tang, H., Lv, Z., Xu, B., Zhou, L., Sun, R., Meng, R., 2023. A spectral-temporal constrained deep learning method for tree species mapping of plantation forests using time series Sentinel-2 imagery. ISPRS J. Photogramm. Remote Sens. 204, 397–420.

Isaienkov, K., Yushchuk, M., Khramtsov, V., Seliverstov, O., 2021. Deep learning for regular change detection in ukrainian forest ecosystem with sentinel-2. IEEE J. Sel. Top. Appl. Earth Obs. Remote Sens. 14, 364–376. https://doi.org/10.1109/jstars.2020.3034186.

Jamali, A., Roy, S.K., Li, J., Ghamisi, P., 2023. TransU-Net++: Rethinking attention gated TransU-Net for deforestation mapping. Int. J. Appl. Earth Obs. Geoinformation 120. https://doi.org/10.1016/j.jag.2023.103332.

John, D., Zhang, C., 2022. An attention-based U-Net for detecting deforestation within satellite sensor imagery. Int. J. Appl. Earth Obs. Geoinformation 107. https://doi.org/10.1016/j.jag.2022.102685.

Karra, K., Kontgis, C., Statman-Weil, Z., Mazzariello, J.C., Mathis, M., Brumby, S.P., 2021. Global land use/land cover with Sentinel 2 and deep learning. IEEE, pp. 4704–4707.

Kleinman, J.S., Goode, J.D., Fries, A.C., Hart, J.L., 2019. Ecological consequences of compound disturbances in forest ecosystems: a systematic review. Ecosphere 10. https://doi.org/10.1002/ecs2.2962.

Le Page, Y., Van Der Werf, G.R., Morton, D.C., Pereira, J.M.C., 2010. Modeling fire-driven deforestation potential in Amazonia under current and projected climate conditions. J. Geophys. Res, G Biogeosciences, p. 115.
Li, L., Long, D., Wang, Y., Woolway, R.I., 2025. Global dominance of seasonality in shaping lake-surface-extent dynamics. Nature 642, 361–368. https://doi.org/10.1038/s41586-025-09046-3.
Li, Z., 2020. Discriminating treed and non-treed wetlands in boreal ecosystems using time series Sentinel-1 data.
Liu, R., Dong, J., Ge, Y., Lin, H., Che, X., Di, Y., Chen, X., Qi, S., Ding, M., Xiao, X., Zhang, G., 2024. Tracking paddy rice acreage, flooding impacts, and mitigations during El Niño flooding events using Sentinel-1/2 imagery and cloud computing.
Liu, Z., Lin, Y., Cao, Y., Hu, H., Wei, Y., Zhang, Z., Lin, S., Guo, B., 2021. Swin transformer: Hierarchical vision transformer using shifted windows. In: Presented at the Proceedings of the IEEE/CVF International Conference on Computer Vision, pp. 10012–10022.
Lu, X., Weng, Q., 2026. Semantic segmentation of single SAR imagery leveraging historical Sentinel-1 and Sentinel-2 data. Int. J. Appl. Earth Obs. Geoinformation 146, 105114.
Masolele, R.N., De Sy, V., Herold, M., Marcos, D., Verbesselt, J., Gieseke, F., Mullissa, A. G., Martius, C., 2021. Spatial and temporal deep learning methods for deriving land-use following deforestation: a pan-tropical case study using Landsat time series. Remote Sens. Environ. 264. https://doi.org/10.1016/j.rse.2021.112600.
McGregor, I.R., Connette, G., Gray, J.M., 2024. A multi-source change detection algorithm supporting user customization and near real-time deforestation detections. Remote Sens. Environ. 308. https://doi.org/10.1016/j.rse.2024.114195.
Md Jelas, I., Zulkifley, M.A., Abdullah, M., Spraggon, M., 2024. Deforestation detection using deep learning-based semantic segmentation techniques: a systematic review. Front. for. Glob. Change 7. https://doi.org/10.3389/ffgc.2024.1300060.
Meng, R., Gao, R., Zhao, F., Huang, C., Sun, R., Lv, Z., Huang, Z., 2022. Landsat-based monitoring of southern pine beetle infestation severity and severity change in a temperate mixed forest. Remote Sens. Environ. 269, 112847.
Meng, R., Wu, J., Schwager, K.L., Zhao, F., Dennison, P.E., Cook, B.D., Brewster, K., Green, T.M., Serbin, S.P., 2017. Using high spatial resolution satellite imagery to map forest burn severity across spatial scales in a Pine Barrens ecosystem. Remote Sens. Environ. 191, 95–109. https://doi.org/10.1016/j.rse.2017.01.016.
Mullissa, A., Reiche, J., Herold, M., 2023. Deep learning and automatic reference label harvesting for Sentinel-1 SAR-based rapid tropical dry forest disturbance mapping. Remote Sens. Environ. 298. https://doi.org/10.1016/j.rse.2023.113799.
Mullissa, A.G., Marcos, D., Tuia, D., Herold, M., Reiche, J., 2020. deSpeckNet: generalizing deep learning-based SAR image despeckling. IEEE Trans. Geosci. Remote Sens. 1–15. https://doi.org/10.1109/tgrs.2020.3042694.
Nogueira Lisboa, S., Grinand, C., Betbeder, J., Montfort, F., Blanc, L., 2024. Disentangling the drivers of deforestation and forest degradation in the Miombo landscape: a case study from Mozambique. Int. J. Appl. Earth Obs. Geoinformation 130. https://doi.org/10.1016/j.jag.2024.103904.
Oktay, O., Schlemper, J., Folgoc, L.L., Lee, M., Heinrich, M., Misawa, K., Mori, K., McDonagh, S., Hammerla, N.Y., Kainz, B., 2018. Attention u-net: Learning where to look for the pancreas. ArXiv Prepr. ArXiv180403999.
Olofsson, P., Foody, G.M., Herold, M., Stehman, S.V., Woodcock, C.E., Wulder, M.A., 2014. Good practices for estimating area and assessing accuracy of land change. Remote Sens. Environ. 148, 42–57. https://doi.org/10.1016/j.rse.2014.02.015.
Pišl, J., Rußwurm, M., Haydn Hughes, L., Lenczner, G., See, L., Dirk Wegner, J., Tuia, D., 2024. Mapping drivers of tropical forest loss with satellite image time series and machine learning. Environ. Res. Lett. 19. https://doi.org/10.1088/1748-9326/ad44b2.
Radeloff, V.C., Roy, D.P., Wulder, M.A., Anderson, M., Cook, B., Crawford, C.J., Friedl, M., Gao, F., Gorelick, N., Hansen, M., 2024. Need and vision for global medium-resolution Landsat and Sentinel-2 data products. Remote Sens. Environ. 300, 113918.
Sagan, V., Maimaitijiang, M., Bhadra, S., Maimaitiyiming, M., Brown, D.R., Sidike, P., Fritschi, F.B., 2021. Field-scale crop yield prediction using multi-temporal WorldView-3 and PlanetScope satellite data and deep learning. ISPRS J. Photogramm. Remote Sens. 174, 265–281. https://doi.org/10.1016/j.isprsjprs.2021.02.008.
Seidl, R., Turner, M.G., 2022. Post-disturbance reorganization of forest ecosystems in a changing world. Proc. Natl. Acad. Sci. 119. https://doi.org/10.1073/pnas.2202190119.
Senf, C., Seidl, R., 2021. Mapping the forest disturbance regimes of Europe. Nat. Sustain. 4, 63–70.
Slagter, B., Fesenmyer, K., Hethcoat, M., Belair, E., Ellis, P., Kleinschroth, F., Peña-Claros, M., Herold, M., Reiche, J., 2024. Monitoring road development in Congo Basin forests with multi-sensor satellite imagery and deep learning. Remote Sens. Environ. https://doi.org/10.1016/j.rse.2024.114380.
Smith, C., Baker, J.C.A., Spracklen, D.V., 2023. Tropical deforestation causes large reductions in observed precipitation. Nature 615, 270–275. https://doi.org/10.1038/s41586-022-05690-1.
Solórzano, J.V., Mas, J.F., Gallardo-Cruz, J.A., Gao, Y., Fernández-Montes de Oca, A., 2023. Deforestation detection using a spatio-temporal deep learning approach with synthetic aperture radar and multispectral images. ISPRS J. Photogramm. Remote Sens. 199, 87–101. https://doi.org/10.1016/j.isprsjprs.2023.03.017.
Stahl, A.T., Andrus, R., Hicke, J.A., Hudak, A.T., Bright, B.C., Meddens, A.J.H., 2023. Automated attribution of forest disturbance types from remote sensing data: a synthesis. Remote Sens. Environ. 285. https://doi.org/10.1016/j.rse.2022.113416.
Sun, R., Zhao, F., Huang, C., Huang, H., Lu, Z., Zhao, P., Ni, X., Meng, R., 2023. Integration of deep learning algorithms with a Bayesian method for improved characterization of tropical deforestation frontiers using Sentinel-1 SAR imagery. Remote Sens. Environ. 298. https://doi.org/10.1016/j.rse.2023.113821.
Tanase, M.A., Ismail, I., Lowell, K., Karyanto, O., Santoro, M., 2015. Detecting and quantifying forest change: the potential of existing C- and X-band radar datasets. PLoS One 10, e0131079. https://doi.org/10.1371/journal.pone.0131079.
Tang, X., Bratley, K.H., Cho, K., Bullock, E.L., Olofsson, P., Woodcock, C.E., 2023. Near real-time monitoring of tropical forest disturbance by fusion of Landsat, Sentinel-2, and Sentinel-1 data. Remote Sens. Environ. 294. https://doi.org/10.1016/j.rse.2023.113626.
Tao, X., Huang, C., Zhao, F., Schleeweis, K., Masek, J., Liang, S., 2019. Mapping forest disturbance intensity in North and South Carolina using annual Landsat observations and field inventory data. Remote Sens. Environ. 221, 351–362. https://doi.org/10.1016/j.rse.2018.11.029.
Tian, Y., Zhao, F., Meng, R., Sun, R., Zhang, Y., Shen, Y., Wang, B., Liu, J., Li, M., 2025. A vision foundation model-based method for large-scale forest disturbance mapping using time series Sentinel-1 SAR data. Remote Sens. Environ. 325, 114775.
Tinker, P.B., Ingram, J.S., Struwe, S., 1996. Effects of slash-and-burn agriculture and deforestation on climate change. Agric. Ecosyst. Environ. 58, 13–22.
Vitale, S., Ferraioli, G., Pascazio, V., 2021. Multi-Objective CNN-Based Algorithm for SAR Despeckling. IEEE Trans. Geosci. Remote Sens. 59, 9336–9349. https://doi.org/10.1109/tgrs.2020.3034852.
Wright, J.S., Fu, R., Worden, J.R., Chakraborty, S., Clinton, N.E., Risi, C., Sun, Y., Yin, L., 2017. Rainforest-initiated wet season onset over the southern Amazon. Proc. Natl. Acad. Sci. U S A 114, 8481–8486. https://doi.org/10.1073/pnas.1621516114.
Ye, S., Rogan, J., Zhu, Z., Eastman, J.R., 2021. A near-real-time approach for monitoring forest disturbance using Landsat time series: stochastic continuous change detection. Remote Sens. Environ. 252. https://doi.org/10.1016/j.rse.2020.112167.
Yu, Y., Ginoux, P., 2022. Enhanced dust emission following large wildfires due to vegetation disturbance. Nat. Geosci. 15, 878–884. https://doi.org/10.1038/s41561-022-01046-6.
Zhang, Y., Ling, F., Wang, X., Foody, G.M., Boyd, D.S., Li, X., Du, Y., Atkinson, P.M., 2021. Tracking small-scale tropical forest disturbances: Fusing the Landsat and Sentinel-2 data record. Remote Sens. Environ. 261. https://doi.org/10.1016/j.rse.2021.112470.
Zhao, F., Sun, R., Zhong, L., Meng, R., Huang, C., Zeng, X., Wang, M., Li, Y., Wang, Z., 2022. Monthly mapping of forest harvesting using dense time series Sentinel-1 SAR imagery and deep learning. Remote Sens. Environ. 269. https://doi.org/10.1016/j.rse.2021.112822.
Zhao, P., Meng, R., Xu, B., Wu, J., Shen, Y., Liu, J., Huang, B., Yin, T., Ferreira, M.P., Zhao, F., 2026. Improved grass species mapping in high-diversity wetland by combining UAV-based spectral, textural. Geometric Measurements. Remote Sens. 18, 927.